

A study of the free tropospheric humidity interannual variability using Meteosat data and an advection-condensation transport model

Hélène Brogniez, Rémy Roca, Laurence Picon

▶ **To cite this version:**

Hélène Brogniez, Rémy Roca, Laurence Picon. A study of the free tropospheric humidity interannual variability using Meteosat data and an advection-condensation transport model. Journal of Climate, 2009, 22 (24), pp.6773-6787. 10.1175/2009JCLI2963.1 . hal-00408503

HAL Id: hal-00408503
https://hal.science/hal-00408503

Submitted on 22 Nov 2020

HAL is a multi-disciplinary open access archive for the deposit and dissemination of scientific research documents, whether they are published or not. The documents may come from teaching and research institutions in France or abroad, or from public or private research centers.

L'archive ouverte pluridisciplinaire **HAL**, est destinée au dépôt et à la diffusion de documents scientifiques de niveau recherche, publiés ou non, émanant des établissements d'enseignement et de recherche français ou étrangers, des laboratoires publics ou privés.

A Study of the Free Tropospheric Humidity Interannual Variability Using Meteosat Data and an Advection–Condensation Transport Model

HÉLÈNE BROGNIEZ

Laboratoire Atmosphères, Milieux, Observations Spatiales, CNRS/IPSL, Vélizy, France

RÉMY ROCA AND LAURENCE PICON

Laboratoire de Météorologie Dynamique, CNRS/IPSL, Paris, France

(Manuscript received 8 December 2008, in final form 25 May 2009)

ABSTRACT

Water vapor in the midtroposphere is an important element for the earth radiation budget. Despite its importance, the relative humidity in the free troposphere is not very well documented, mainly because of the difficulties associated with its measurements. A new long-term archive of free tropospheric humidity (FTH) derived from the water vapor channel of the Meteosat satellite from 1983 to 2005 is introduced. Special attention is dedicated to the long-term homogeneity and the definition of the retrieval layer. It is shown to complement the existing databases and is used to establish the climatology of FTH. Interannual variability is then evaluated for each season by using a normalized interannual standard deviation. This normalization approach reveals the importance of the relative variability of the dry areas to the moist regions. In consequence, emphasis is on the driest area of the region. Focusing on composites of the moist and dry seasons of the time series, the authors demonstrate that the 500-hPa relative humidity field, reconstructed using an idealized Lagrangian model, is a good proxy for the FTH variability there. The analysis of the origin of the air mass, using the back trajectory model, points out that lateral mixing between the deep tropics and extratropical latitudes takes place over this area, as advocated in previous theoretical studies. Systematic estimation of this large-scale mixing shows that, indeed, a significant part of the interannual variability of the free tropospheric humidity in this subtropical region stems from the amount of mixing of air originating from the deep tropics versus extratropical latitudes. The importance of this mechanism in the general understanding of the FTH distribution and variability is then discussed.

1. Introduction

Water vapor is known to be a fundamental component of the earth radiative budget through a strongly positive feedback loop with the surface temperature (e.g., Manabe and Wetherald 1967; Bony et al. 2006). Water vapor in the mid- to upper troposphere, while representing a small fraction of the total column, has a significant impact on the outgoing longwave radiation (OLR), the sensitivity of which increases with dryness of the free troposphere (e.g., Pierrehumbert 1995; Spencer and Braswell 1997; Pierrehumbert et al. 2007). Documenting and understanding the distribution and variability of humidity is thus critical for assessing current climate and climate change simulations on a sound physical basis.

In the tropical boundary layer, the water vapor distribution is directly influenced by surface evaporation, itself influenced by the surface temperature, yielding to strong correlations at monthly and interannual scales between water vapor and the SST patterns (e.g., Stephens and Greenwald 1991). At intraseasonal scales, the large-scale convergence/transport of moisture needs to be invoked to complete the picture; a typical example of this being the short-term variability of the monsoonal flux observed in West African and Indian monsoon systems (Bock et al. 2007; Bhat 2006). At even smaller scales, such as the convective event scale, cloud physics needs to be incorporated to explain the water vapor variability, such as the strong drying associated with the passing of an organized system (e.g., Redelsperger et al.

Corresponding author address: Hélène Brogniez, Laboratoire Atmosphères, Milieux, Observations Spatiales, 10-12 avenue de l'Europe, 78140 Vélizy-Villacoublay, France.
E-mail: helene.brogniez@latmos.ipsl.fr

DOI: 10.1175/2009JCLI2963.1

© 2009 American Meteorological Society

Downloaded from http://journals.ametsoc.org/jcli/article-pdf/22/24/6773/3951994/2009jcli2963_1.pdf by guest on 22 November 2020

2002), without mentioning the subcloud scales where microphysics drive the evaporation in the downdrafts (e.g., Emanuel 1991). In the free troposphere, on the other hand, over large portions of the subtropics, the distribution of water vapor is controlled by large-scale transport and the temperature at which the last saturation of the air mass occurred (Pierrehumbert 1998). There, evaporation from clouds has been shown to be negligible (Sherwood 1996; Pierrehumbert and Roca 1998; Sherwood and Meyer 2006). In the deep tropics, free tropospheric humidity is more directly influenced by convective system detrainment (e.g., Udelhofen and Hartmann 1995; Salathé and Hartmann 1997; Luo et al. 2007; Chung et al. 2007; Sohn et al. 2008; Tian et al. 2004). Understanding the variability of moisture in the mid- to upper troposphere in the intertropical belt hence requires investigating the transport of water vapor and its variability as well as the variability in the location of deep convection. The signature of multiple intraseasonal modes has, indeed, been reported in the mid- to upper tropospheric humidity in the tropics with periods of 30–60 days (Madden–Julian oscillation) and 10–20 days linked to monsoon onsets and breaks (e.g., Mote et al. 2000; Sassi et al. 2002; Zhan et al. 2006). At these intraseasonal scales in the deep tropics large-scale transport explains some observed dry spells (Roca et al. 2005a), while the occurrence of moistening events are more related to deep convective events (e.g., Roca et al. 2002). At interannual scales, El Niño events are well related with the variability of free tropospheric relative humidity over the Pacific Ocean through both convective pattern shifts and large-scale dynamics modification (Bates et al. 2001; McCarthy and Toumi 2004; Luo et al. 2007). The El Niño response fades away from the Pacific Ocean to other tropical regions where the interannual variability is not well-documented nor understood. In the present study, an attempt is made to document and investigate the mechanisms implied in the interannual variability of the free tropospheric humidity over the tropical Atlantic/Africa region.

Despites its importance to the physics of climate, the distribution of humidity in the tropical free troposphere is not well observed at long-term, interannual, seasonal, intraseasonal, and shorter scales. Indeed, conventional radiosondes, beyond scarcity issues in the tropics, are well known to suffer from biases in upper-tropospheric environmental conditions, which are difficult to correct (Elliot and Gaffen 1991; Soden and Lanzante 1996). Atmospheric reanalyses also suffer from spurious behavior at the extremes of the range of relative humidity, and the time-varying assimilation procedure might contaminate their description of the interannual variability (Allan 2006). Satellite estimates are a good alternative to document the variability of the relative humidity of the free troposphere. Infrared radiometers, onboard meteorological satellites since the late 1970s, routinely observe water vapor in the strong rotation vibration band, potentially yielding a rich long-term database. These archives are affected by two main limitations though. First, the long-term variability can be corrupted by change of the captor over time and variation in the absolute calibration (e.g., Picon et al. 2003). Second, the radiance field is not directly related to a simple estimate of the relative humidity and is usually associated with the average clear sky relative humidity over a poorly located broad layer of the free troposphere, yielding to some uncertainty in the retrieval (e.g., Fischer et al. 1981; Schmetz and Turpeinen 1988; Soden and Bretherton 1993; Bates et al. 2001; Roca et al. 2003; Brogniez et al. 2004). Here, an extended long-term archive of humidity estimates built from the Meteosat observations is used to document the variability of the relative humidity in the free troposphere. The emphasis is put on the quality of the retrieval and the definition of the atmospheric layer, as well as on stability over time.

The mechanisms that control the relative humidity distribution in the subtropical midtroposphere are threefold: subsidence, which brings down dry air from aloft; lateral mixing, which brings in moistened air from the deep convective regions; and drying by processing of air through the cold extratropics (Pierrehumbert 1998). While the first two mechanisms have received much attention and have been incorporated in successful simple theoretical models of the subtropical humidity distribution (e.g., Pierrehumbert 1999; Mapes 2001; Pierrehumbert et al. 2007; Sherwood et al. 2006; Ryoo et al. 2008), the last one has yet to be addressed in these idealized frameworks. As an incentive to do so here, the relative importance of lateral mixing of tropical and extratropical air is shown, using an advection–condensation model, to explain the FTH interannual variability over a key dry region of the subtropics.

The paper is organized as follows. Section 2 briefly presents the Meteosat database of free tropospheric humidity estimated from the 6.3-μm measurements; details of the database production are shown in two appendices. The FTH climatology is then shown in section 3 together with some elements characterizing its interannual variability. Section 4 is dedicated to the study of the link between the satellite measurements and the large-scale dynamics. Discussions and perspectives are provided in the concluding section.

2. Data

The data used in this study covers the 1983–2005 period of observations of the Africa/tropical Atlantic

Downloaded from http://journals.ametsoc.org/jcli/article-pdf/22/24/6773/3951994/2009jcli2963_1.pdf by guest on 22 November 2020

atmosphere by the first generation Meteosat satellites (Meteosat-2 to -7). Water vapor (WV) brightness temperature (BT) in the 6.3-μm, so-called water vapor, channel are available at a 3-hourly time step and an equivalent resolution of 30 km through the International Satellite Cloud Climatology Project (ISCCP) (Rossow and Schiffer 1991). Homogenization of this long time series of WV measurements, covering six radiometers, has been performed following Picon et al. (2003); the main aspects are detailed in appendix A. The water vapor clear-sky radiances (CSR) are obtained using the scene selection methodology described in Brogniez et al. (2006), based on the ISCCP-DX cloud products: in addition to the clear-sky-only pixels, low-level clouds with a cloud-top pressure greater than 680 hPa are kept in the database, improving significantly the sampling of the region over a season. Thus, for the subtropical regions up to 80% of scenes are kept over the course of a season, versus about 50% in the clear-sky-only selection [see Brogniez et al. (2006) for details].

The free tropospheric humidity quantity is estimated directly from the CSR using a simplified theory of the radiative transfer and the thermodynamical properties of an idealized tropical profile (Soden and Bretherton 1993; see appendix B for details in the method). The use of the local relative humidity Jacobian [∂BT/∂RH, provided by the Radiative Transfer for the TIROS Operational Vertical Sounder (RTTOV) fast radiative code] for the determination of the layer of influence of the water vapor BT has been preferred over other vertical operators (cf. appendix B). Such interpretation of the BT yields a small retrieval bias (-0.21%) and a small rms error (1.47%), reducing by a factor of 2 the two uncertainties of similar products traditionally quoted in the literature (Brogniez et al. 2004). Therefore, we interpret the water vapor BT as the free tropospheric humidity (FTH), which better corresponds to the region of influence of the local Jacobian over the intertropical belt than the frequently used upper-tropospheric humidity term (Roca et al. 2003; Brogniez et al. 2004, 2005). Evaluation of the Meteosat FTH database against estimates of FTH from radiosonde observations (cf. appendix B) over the entire period reveals a small bias of -1.23%, stable over the long 1984–2005 period ($\sigma = 1.70\%$).

3. Climatology

a. Mean seasons

The Meteosat-derived climatology for each season (Fig. 1) is similar to that observed by radiosondes and in situ measurements (e.g., Peixoto and Oort 1996; Luo et al. 2007) and reported from a shorter study using Meteosat (Picon et al. 1995; Schmetz et al. 1995) and other radiometer measurements, such as the High Resolution Infrared Radio Sounder (HIRS-12) (Stephens et al. 1996; Bates et al. 2001; McCarthy and Toumi 2004) and the Atmospheric Infrared Sounder (AIRS) onboard the *Aqua* satellite (Gettelman et al. 2006). Among the large patterns the moist ITCZ, reaching values of FTH around 50%, is clearly seen with its position shifting from 10°S over the African continent in December–February (DJF), Fig. 1a, to about 10°N over the West African region area in June–August (JJA), Fig. 1c. In both parts of the ITCZ, broad regions corresponding to subsidence branches of the circulation cells, with FTH values less than 15%–20% widening and drying over the course of the year, reach less than 10% in June–August in both hemispheres (Fig. 1c). Over the Eastern Mediterranean in boreal summer the FTH reaches its climatological minimum with values as low as 7%–8%.

b. Interannual variability

Figure 2 shows the interannual standard deviation of the seasonally averaged FTH for the four seasons as a proxy to document the interannual variability. Generally, the patterns of large variability are located in the moist areas and on the edges of the ITCZ, while less variability characterizes the dry areas of the subtropics. The magnitude of this standard deviation varies between 7% and 2%. In winter standard deviations are larger than in summer and other seasons. The variability is further analyzed using computations of the coefficient of variation σ_n (standard deviation normalized by the mean). Here σ_n is better suited to document the key role of those extremely dry areas for the earth's radiative budget. Indeed, the sensitivity of OLR to the FTH is first dependent upon the background profile. Radiative transfer computations indicate that OLR is three times more sensitive to a given perturbation of relative humidity in a dry, rather than moist, environment (Spencer and Braswell 1997; Udelhofen and Hartmann 1995; Roca et al. 2002; Sohn and Schmetz 2004). In other words, a small absolute variation in dry conditions can yield a significant OLR impact similar to the large absolute value associated with a moist environment. The maps in Fig. 3 reveal that, while large values are overall still found in winter, the location of large relative variability is shifted toward the gradient areas between moist and very dry air as well as over the dry areas. In summer, the Eastern Mediterranean region, previously a low interannual variability area, now stands out as the region with more important normalized variability, with values in excess of 25%. Similarly the ITCZ region exhibits small interannual variability with $\sigma_n \sim 5\%$. To further support the importance of analyzing the normalized interannual variability, the sensitivity computations

Downloaded from http://journals.ametsoc.org/jcli/article-pdf/22/24/6773/3951994/2009jcli2963_1.pdf by guest on 22 November 2020

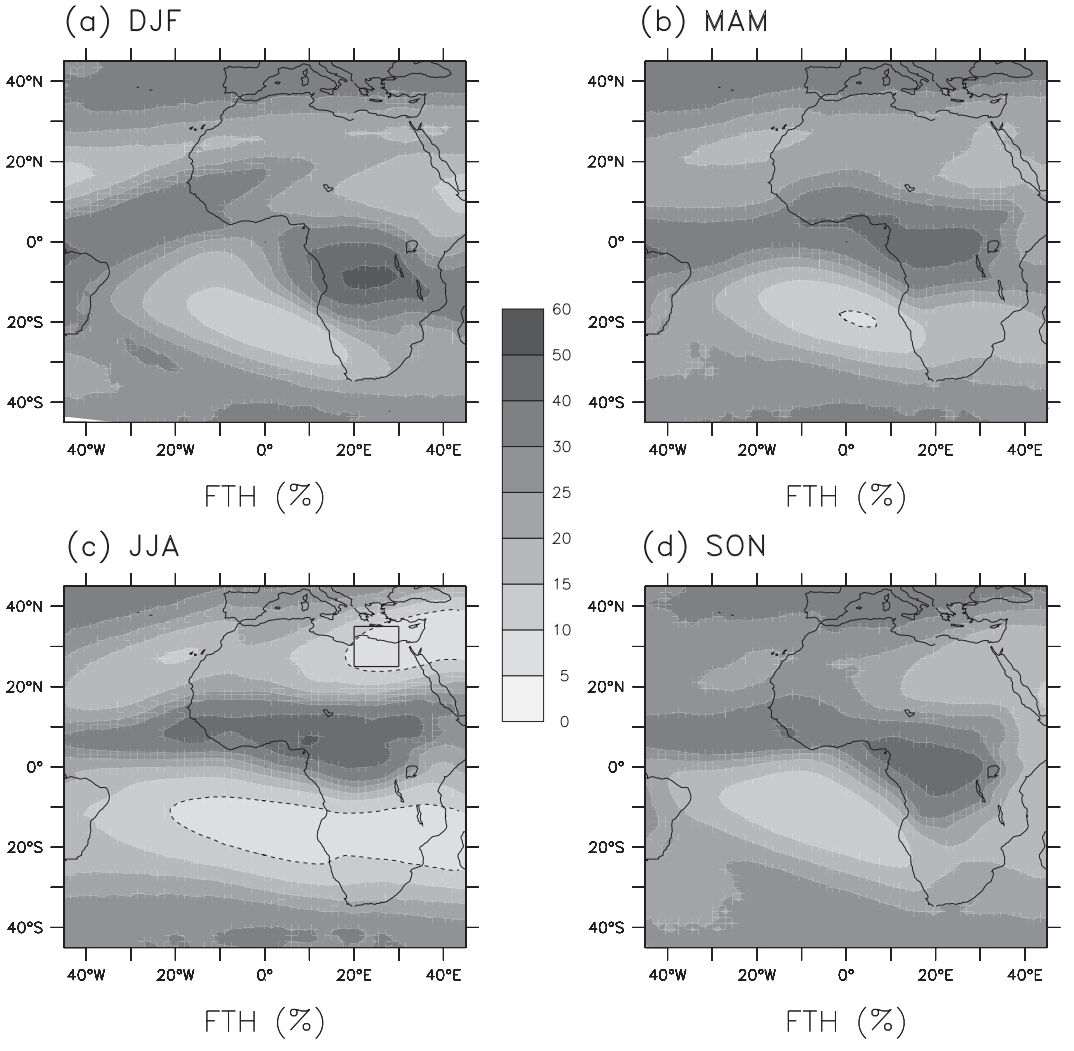


FIG. 1. Mean seasonal cycle of the Meteosat-derived FTH (%) over 1984–2004 for (a) December–February, (b) March–May, (c) June–August, and (d) September–November. The box limits the selected area of study: (c) the Eastern Mediterranean region (25°–35°N, 20°–30°E). The dashed line limits the ≤10% FTH areas.

of Spencer and Braswell (1997) have been replicated using the CRM model (e.g., Zender 1999) in the configuration detailed in Roca et al. (2005b), allowing us to evaluate this normalizing effect on OLR. In typical tropical temperature conditions, holding temperature constant and changing the FTH from 10% to 7.5% (equivalent to a 25% relative decrease) would increase OLR by 4.4 W m^{-2}, from 315.3 to 319.7 W m^{-2}. In ITCZ-like conditions (FTH ~ 50%), reducing the FTH by a quarter would yield to a similar increase in OLR by around 6 W m^{-2}. If the climatological observed interannual variability in these regions (5%) is used instead, the increase in OLR is only 1.4 W m^{-2}. This recalls the importance of small absolute variations that can be significant relative variations in a dry environment. In summer, the region of the Eastern Mediterranean Sea reveals very dry subtropical climatological values, as well as enhanced interannual relative variability, of importance to the radiative budget. Hence, we document next in more detail this outstanding limited area.

c. The Eastern Mediterranean region in summer

In the rest of the paper, the seasonal average over July and August (JA) is preferred over the JJA period in order to account for the data availability discussed in section 2. Note that none of the following conclusions are modified by using JJA, but using JA slightly enhances the results significance. The Eastern Mediterranean region (25°–35°N, 20°–30°E) is characterized by a dry summer averaged FTH (8.3%) and a large normalized interannual variation (25.7%).

Downloaded from http://journals.ametsoc.org/jcli/article-pdf/22/24/6773/3951994/2009jcli2963_1.pdf by guest on 22 November 2020

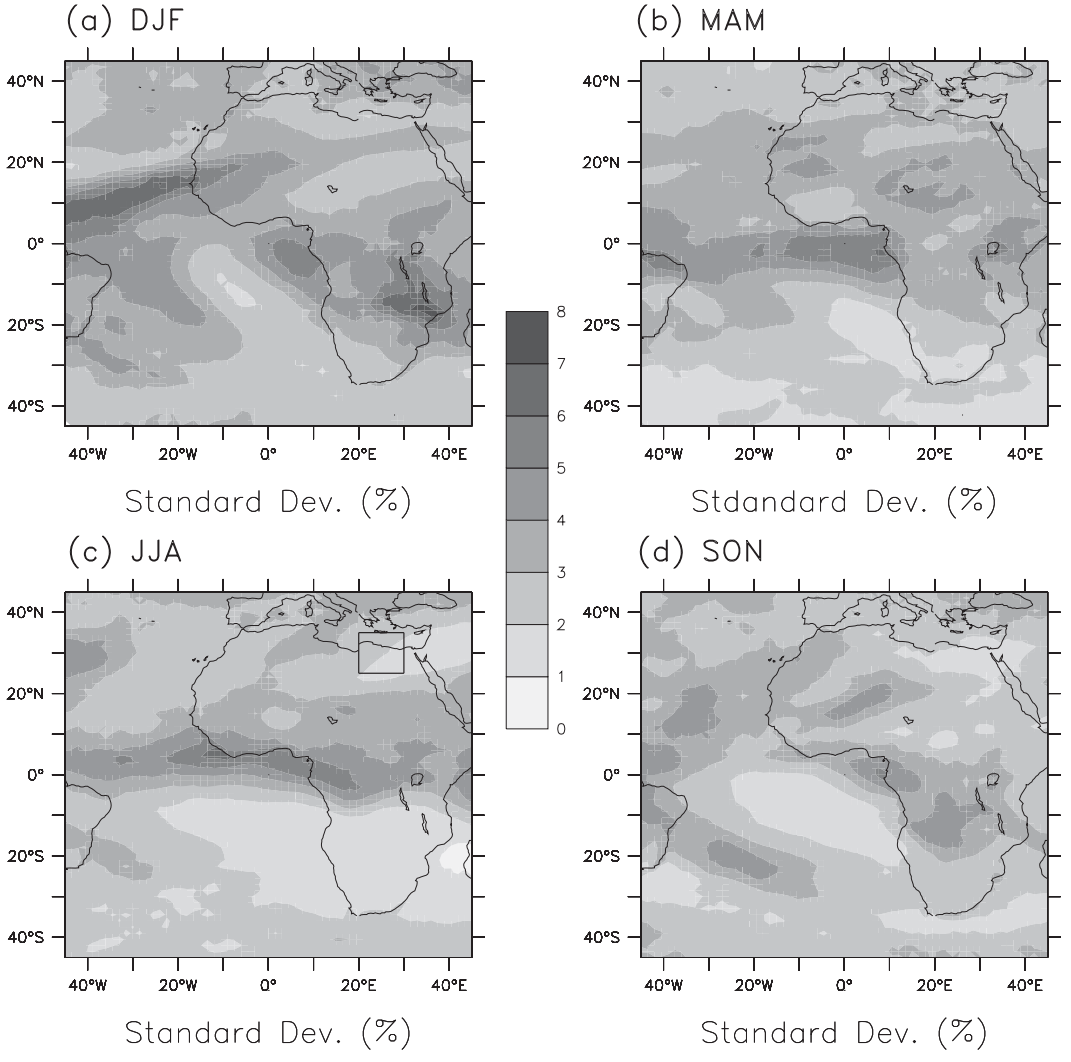


FIG. 2. Interannual standard deviations of the FTH (%) observed by METEOSAT over 1984–2004: (a) December–February, (b) March–May, (c) June–August, and (d) September–November.

Figure 4 summarizes some statistics of the FTH for this region over the period studied using box-and-whiskers plots. Computations were performed using daily averaged FTH estimates. Beyond the seasonal mean, the main characteristics of the probability distribution functions are given (median, extremes, and quartiles) to characterize the variability. The focus is on years 1984 and 1992, which belong to the driest and less dry years of the period, and shows contrasting statistics over this region. Previous analysis using a preliminary version of this dataset also identified these two years as representative of extreme conditions over the area (Brogniez et al. 2005). Indeed, in 1984, the FTH averages to 5.5% with a median of 5.1% and a small standard deviation of 2.4% (43% in relative terms) and a very dry low first quartile value of 3.5% and a less high value of 6.8% for the third quartile. This is characteristic of a very dry year with steady dry conditions throughout the season. On the other hand, 1992 is characterized by the less moist average of 7.9% and similar relative standard deviation of 37% with maximum values up to 16.2%, indicative of overall moister conditions as well as a more variant moist environment all through the season. This region is further characterized by a relatively small variation of the temperature field in the midtroposphere. The National Centers for Environmental Prediction–National Center for Atmospheric Research (NCEP–NCAR) 40-yr reanalyses (Kalnay et al. 1996) average temperature at 500 hPa is 266.5 K with an interannual standard deviation of 1.4 K, a 0.5% relative variation. Such variations in the temperature are unlikely of provoke large variations in the relative humidity (e.g., Peixoto and Oort 1996). In

Downloaded from http://journals.ametsoc.org/jcli/article-pdf/22/24/6773/3951994/2009jcli2963_1.pdf by guest on 22 November 2020

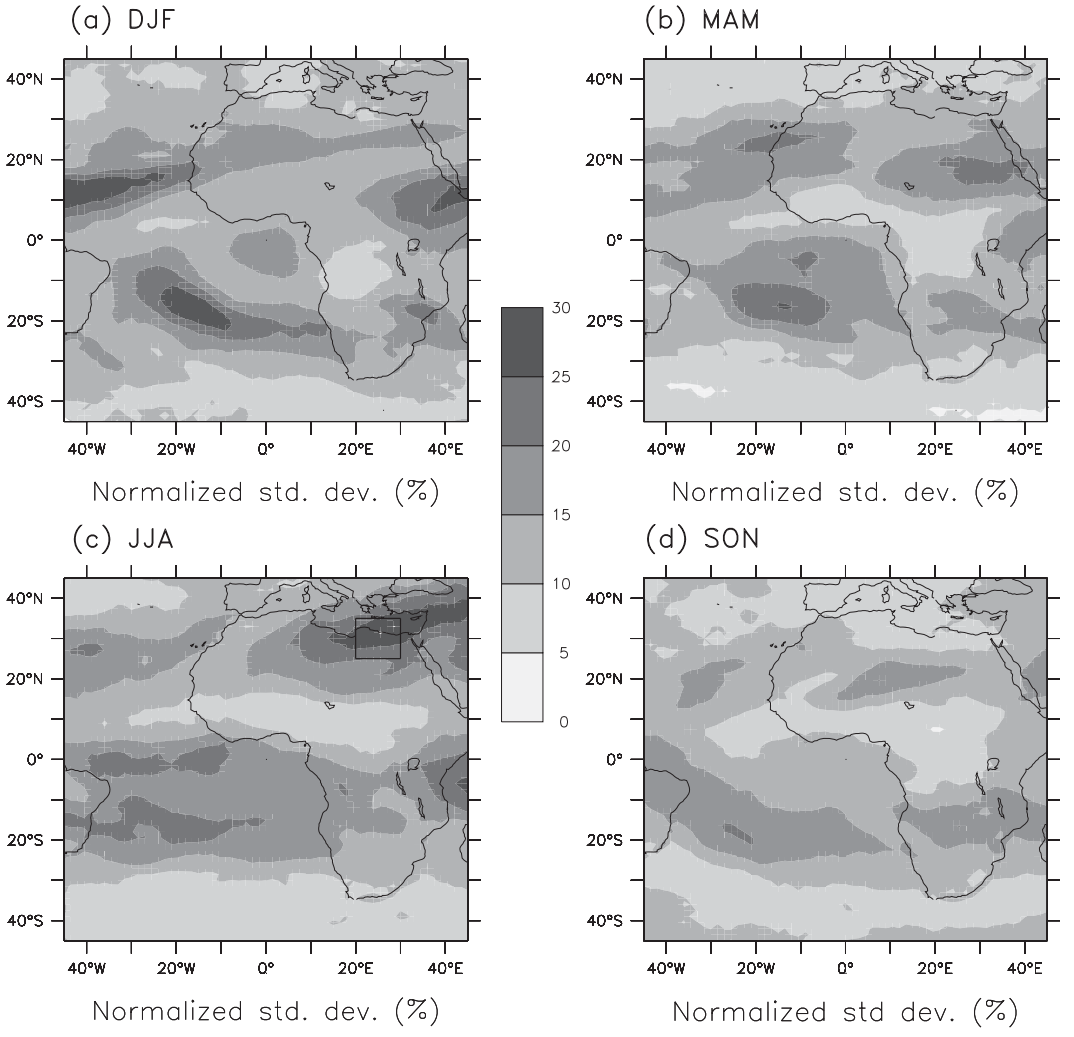


FIG. 3. As in Fig. 2 but for the normalized standard deviation (%).

1984, the July–August 500-hPa temperature averages 267 K and 267.1 K in 1992. This indicates that the temperature influence on the interannual variability of FTH there can be ruled out and that the differences in humidity between these two extreme years are likely contributed by moisture variations. To add significance to the results, we discuss in the following the behavior of the composites of the extreme years of the period: the three moistest years (1987, 1988, and 1992) and three driest years (1984, 1985, and 2000).

4. Large-scale transport and variability of the FTH

The FTH corresponds to the vertical average of relative humidity using a Jacobian function to weight the contribution from different levels. As a result, neither a single level of the atmosphere nor a simple combination of many easily matches the FTH. When considering the *relative* variability in space and time of FTH, so, without looking for strong linear relationship, one can expect that the study of relative humidity at a single level could enlighten our understanding of variability of the satellite integrated product. We show next that, indeed, the relative humidity field at 500 hPa computed with an idealized advection–condensation transport model is a reasonable proxy for studying the variability of FTH in the dry region of interest.

a. A Lagrangian transport model for water vapor

The model belongs to the class of the last-saturation models: at a given point in time and space, the water vapor mixing ratio of an air parcel corresponds to the minimum mixing ratio encountered along its trajectory. This position of last saturation hence depends only on the atmospheric circulation and the temperature field. Water vapor is considered as a nondiffusive tracer,

Downloaded from http://journals.ametsoc.org/jcli/article-pdf/22/24/6773/3951994/2009jcli2963_1.pdf by guest on 22 November 2020

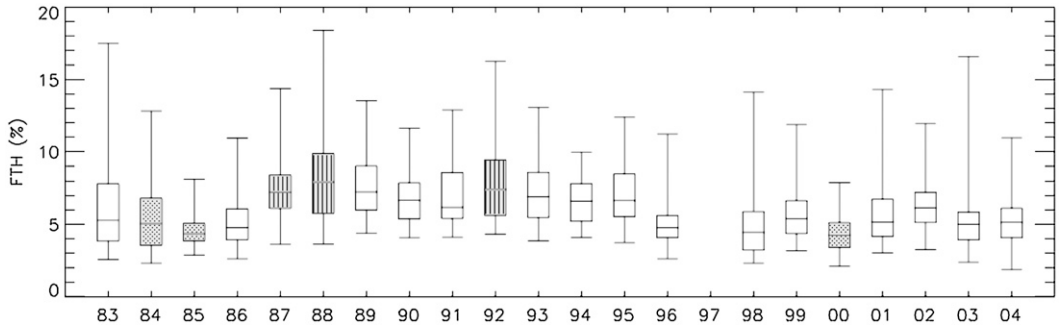


FIG. 4. Box plots of the FTH estimated by Meteosat defined for each July–August over the Eastern Mediterranean area (25°–35°N, 20°–30°E). The box is characterized by the median, the first and third quartiles, and the whiskers represent the minimum and maximum values. Also indicated are the three driest years (dotted pattern) and the three moistest years (vertical pattern).

which suppresses the mixing of moisture among air masses, caused for instance by diffusion from small-scale turbulence. Finally, the precipitation efficiency is assumed to be 100%, thus simplifying microphysical processes: the model ignores the redistribution of excess moisture that condensates as the air parcel penetrates a subsaturated environment. This model is described at length by Pierrehumbert (1998) and Pierrehumbert and Roca (1998). It is used in the same configuration as in Roca et al. (2005a), Brogniez and Pierrehumbert (2006), and in Pierrehumbert et al. (2007). The three components of the wind (u, v, ω) as well as the air temperature field are taken from the 6-hourly NCEP reanalyses provided on a regular 2.5° latitude × longitude grid. The only source of moisture is the saturated planetary boundary layer defined at the 850 hPa, whereas the sink is the precipitation field from NCEP used to diagnose deep convection based on a threshold of 5 cm day^{-1}. The relative humidity of the air parcel is computed with respect to water using the water vapor mixing ratio of the last saturation and the NCEP air temperature. For our purpose, reconstruction of the relative humidity field is performed at the 500-hPa pressure level (hereafter RH_{500}), on a 0.5° grid and the trajectories are integrated over 12.5 days backward in time or until the air mass encounter deep convection. Roca et al. (2005a) showed that, over dry regions of the Sahel, the reconstructed RH_{500} agrees within 10% with observed RH_{500} from radiosondes and are consistent over the entire African subsidence regions (see also Pierrehumbert 1998; Pierrehumbert and Roca 1998). The model is integrated for all summer seasons of the 1983–2004 period of study.

b. Results for dry and moist extremes composites

As shown in the previous section, over the Eastern Mediterranean region, the 1984, 1985, 2000 seasons belong to the driest July–August seasons of the period while 1987, 1988, 1992 are among the wetter seasons. These extreme years have been selected to illustrate the usefulness of the reconstructed relative humidity at 500 hPa as a proxy for FTH at the interannual scale and are used to composite a significant dry season and significant moist season. Figure 5 shows the associated FTH and RH_{500} maps. While the overall FTH patterns are similar, the dry composite is characterized by a large very dry area spreading over the Eastern Mediterranean region up to the eastern border of our domain of study, which is not seen in the moist composite. This interannual contrast is captured in the reconstructed relative humidity field with a dry pattern of RH_{500} below 5% only observed in the dry case. Maps of relative humidity at 500 hPa from the NCEP2 reanalysis and from the 40-yr ECMWF Re-Analysis (ERA-40, not shown) also confirm these differences between the two seasons.

Beyond agreement between the proxy and FTH on the differential seasonal average in between theses extreme years, relative humidity also captures some of the variability of the FTH at smaller scales. As shown in Fig. 4, in addition to being dryer, the dry years appears much steadier than in the moist composite, with smaller differences between the first and third quartiles and smaller maximum values (except for 1984), suggesting the presence of some moist plumes during the moist years over the region. The same computations have been repeated for the daily 500-hPa relative humidity (not shown) and show that, similarly, the relative humidity intraseasonal variation is smaller during the dry composite compared to the moist composite. However, the magnitude is larger in the case of a single level than for the FTH product, as expected from the broad vertical averaging associated to the latter. Recall that one is not looking for any linear relationship between FTH and relative humidity but for an agreement in their *relative* variability. Indeed, at the interannual scale and when

Downloaded from http://journals.ametsoc.org/jcli/article-pdf/22/24/6773/3951994/2009jcli2963_1.pdf by guest on 22 November 2020

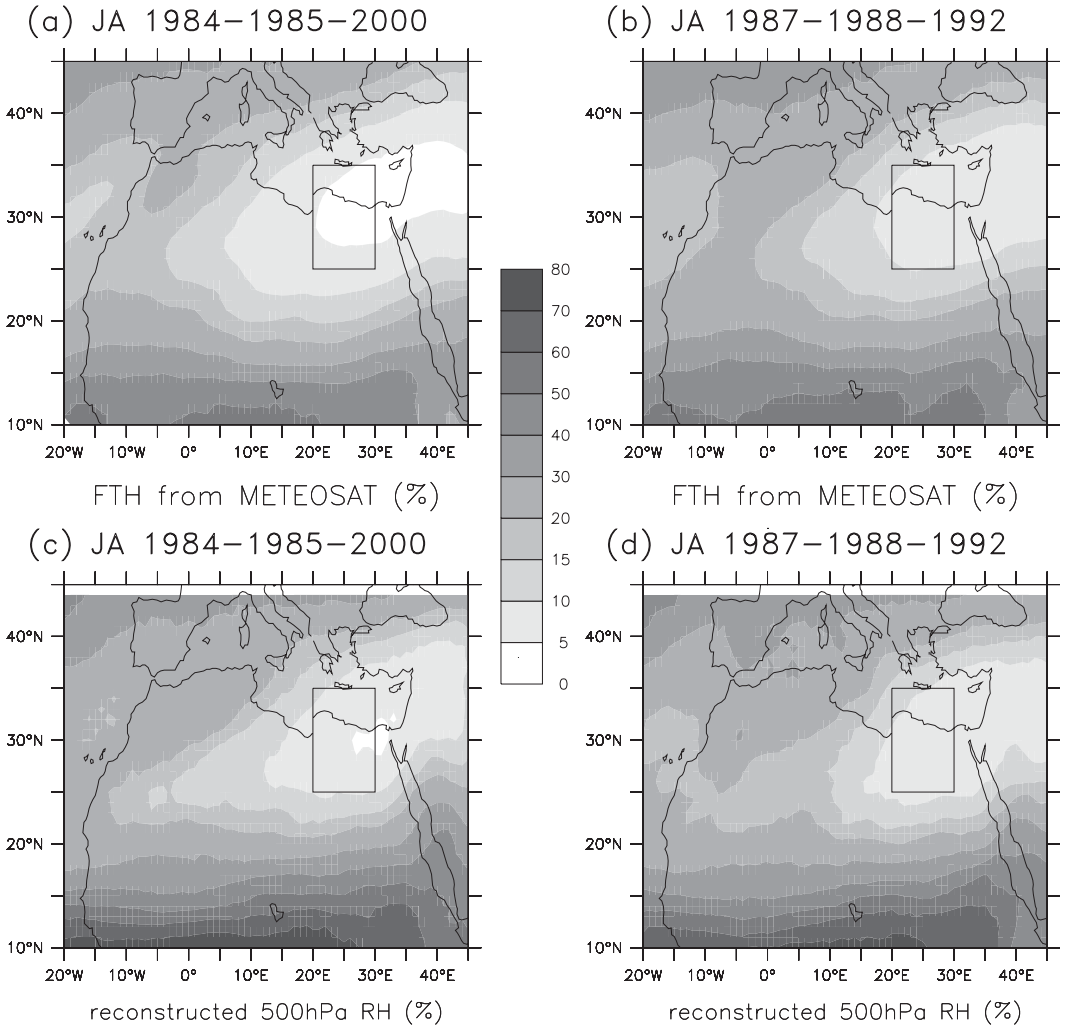


FIG. 5. Maps of (a),(b) observed FTH from Meteosat and (c),(d) the reconstructed 500-hPa relative humidity from the back-trajectory model for the composites (left) July–August 1984, 1985, 2000 and (right) July–August 1987, 1988, 1992.

considering both the mean and variability within each season, the variability of the recomputed relative humidity corresponds well to the variability observed in FTH, permitting use of the former as a good proxy of the latter at the scales considered.

The results of the validated model are now used to identify the origin of the dry/moist air. Figure 6 shows a latitude–altitude diagram of the zonally accumulated density of the last-saturation coordinates (Roca et al. 2005a) for the air masses arriving over the Eastern Mediterranean area for the two years. Both seasons reveal a generally similar pattern. Last saturation occurred over a broad layer of the free troposphere with saturation pressure ranging from 400 to 150 hPa and spread over the Northern Hemisphere. Two cores of frequent locations of the last saturation are also well defined: from 10° to 20°N and ~150 to 325 hPa and a larger one located from 40° to 60°N spanning the 200–350-hPa region. A third region of interest corresponds to the lowest levels, from 350 to 450 hPa, of the two regions. For the dry composite, the tropical core is the main contributor to the seasonal average closely followed by the extratropical core and is located in the upper troposphere. In the moist case, on the other hand, the extratropical core is the most important contributing region. The lowest part of the region also contributes more so than in the dry case. The zonally averaged temperature (averaged over a large zonal domain where the actual saturation took place) is also shown in Fig. 6. There is hardly any difference between the temperature distribution of the extremes in both the vertical and in latitude. The two latitudinal regions are characterized by a similar distribution of

Downloaded from http://journals.ametsoc.org/jcli/article-pdf/22/24/6773/3951994/2009jcli2963_1.pdf by guest on 22 November 2020

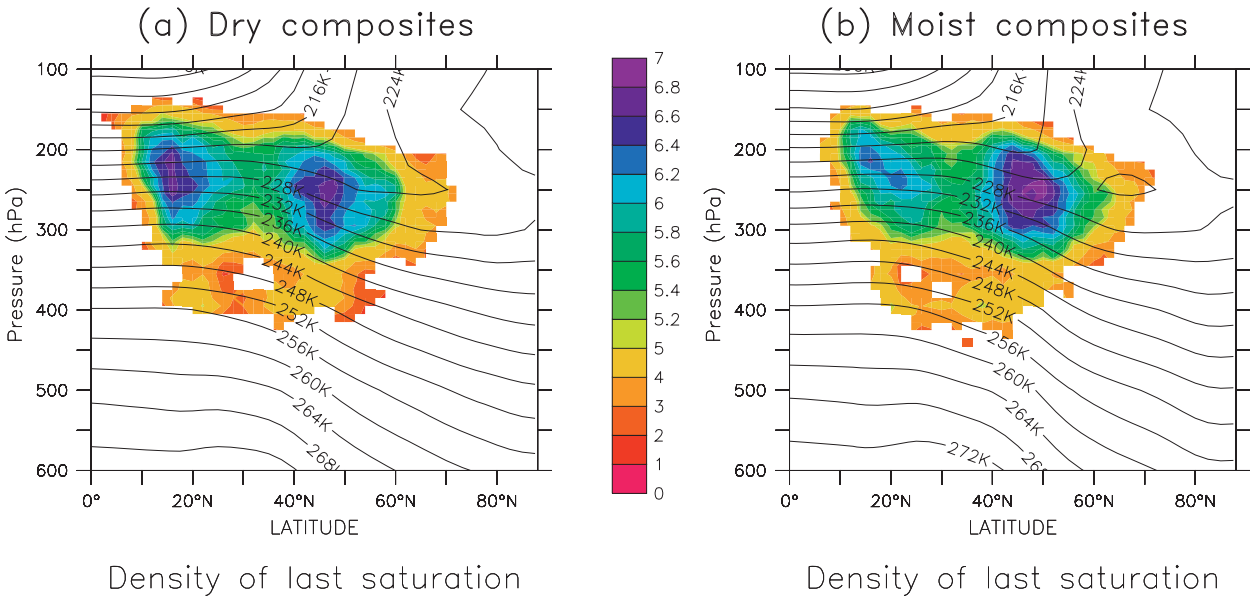


FIG. 6. Zonally and temporally integrated distributions (in natural log scale) of airmass last-saturation positions for the July–August (a) dry and (b) moist composite. Contours are for the mean air temperature from the NCEP reanalyses averaged over 60°W–40°E for the same periods.

temperature in the upper part. In the 10°–20°N band, where the tropical core is located, the temperature ranges from 212 K at 175 hPa to 244 K at 325 hPa. In the extratropical region at 200 hPa, temperature warms from 220 K to around 224 K over the 40°–60°N band and increases to 240 K at 350 hPa. The upper part of the tropical core is associated more with lower temperature than its extratropical equivalent. In the contributing sector with the lowest levels, over both regions, air masses experience higher temperature than in the cores (240–258 K). Hence, the air that originates from the tropical core is likely to be drier than the one originating from the extratropical regions, itself drier than the lowest level of the tropical region. If the JJA period is used instead of the JA averages, the results are basically unchanged although the overall agreement with the recomputed RH at 500 hPa is slightly less good.

In summary, there is evidence of lateral mixing occurring during these two seasons and the temperature field does not show any large variability that could explain the difference in relative humidity at the interannual scale. Indeed, it is the relative contribution from the different preferred locations, each characterized by a different thermal environment, to the last-saturation statistics that seems to explain the difference in humidity between these extreme years.

c. *Interannual variability*

The previous analysis is now systematized to the whole time series. One index of lateral mixing is built using the back-trajectory model as the fraction of air masses that originate from the deep tropics. Following the previous subsection analysis, the deep tropics are defined as within a 25°N latitude cut off. Another index is used to describe synthetically the interannual variability of the relative humidity in the area. It is the fraction over the area of grid point with RH below 10%. The results below are not sensitive to small changes to the arbitrary thresholds. Figure 7 shows a scatter diagram of these two indices indicated by the year. As expected, the moist 1992 and dry 1984 seasons are plotted as the extremes on the diagram. The relationship between the two indices is almost monotonic with increasing fraction of tropical air associated with a drying of the area. The linear correlation between the two variables is 0.68, significant at the 99% level following a Student-*t* test. When the analysis is repeated considering the JJA season instead of JA, the computations yield similar conclusions with a slightly lower correlation of 0.6. A substantial part of the interannual variability of the relative humidity at 500 hPa is hence explained by the lateral mixing. This indicates that large-scale dynamics, through extratropical versus tropical airmass transport, drives the relative humidity variability over this region. At the scales considered, RH_{500} is a reasonable proxy for the FTH. Although the FTH spreads over multiple levels in the free troposphere, rather than just one, it is likely that the lateral mixing is at play not only at 500 hPa but at other free-tropospheric levels relevant to FTH (e.g., Pierrehumbert and Roca

Downloaded from http://journals.ametsoc.org/jcli/article-pdf/22/24/6773/3951994/2009jcli2963_1.pdf by guest on 22 November 2020

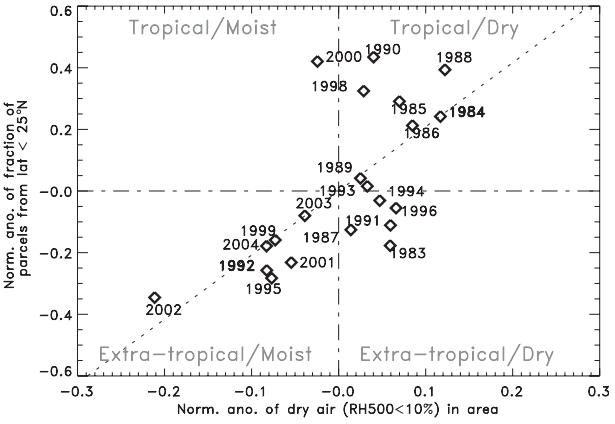


FIG. 7. Plot of the normalized anomaly of the fraction of air masses with a tropical last-saturation position (latitude $< 25°$N) vs the normalized anomaly of dry air (defined by RH $< 10\%$) for the area 25°–35°N, 20°–30°E during each July–August.

1998). Therefore, the mechanism highlighted here for one level should hold for the FTH as well.

5. Summary and discussions

A new long-term archive of free tropospheric humidity derived from Meteosat measurements spanning the 1983–2005 period is introduced. It is based on an extended clear-sky radiance archive previously released and on the climatology of a simplified thermal vertical structure parameter of the tropical atmosphere extracted from the NCEP reanalysis. Comparison with radiosonde-derived FTH shows remarkable stability of the difference between the satellite and in situ estimates over time, giving strong confidence on the former to characterize the FTH variability. The multiyear season averages are presented and show the well-known features of the free tropospheric humidity climatology. The interannual variability is then documented by looking at the interannual standard deviation for each season as well as at the coefficient of variation. In brief, the analysis indicates that

- the absolute interannual variability is dominated by the signal of the moistest region;
- the *relative* interannual variability is more relevant to the OLR variability;
- the dry areas exhibit much more *relative* interannual variability than the moist areas; and
- during the summer, this *relative* variability reaches up to 25% over the Eastern Mediterranean dry zone compared to only 5% over the ITCZ region.

To interpret the reason for this high relative variability over the dry subtropical zone, the analysis is focused on the Eastern Mediterranean region. A Lagrangian transport model, run with the NCEP-reanalyzed 4D winds and temperature fields, is used to compute the relative humidity at 500 hPa and is compared to the FTH. In brief, our findings show that

- the reconstructed 500-hPa RH field is a good proxy to characterize the FTH variability despite the latter corresponding to an elaborated average of multiple levels in the free troposphere,
- Lateral mixing between tropical and extratropical regions is a major feature of this limited area, and
- a significant part of the interannual variability of the free tropospheric humidity in this region of the subtropics stems from the amount of mixing of air originating from the deep tropics versus extratropical latitudes.

This is a somewhat different perspective compared to previously published studies. Bates et al. (2001) indentified a westerly duct swing process associated with large-scale dynamics modifications associated to El Niño, which do not seems to be relevant for our region as discussed above. McCarthy and Toumi (2004), on the other hand, reported an important role of the temperature anomaly in explaining a large portion of the HIRS/UTH interannual variability again with a strong response in the Pacific Ocean. The local temperature interannual variability could, indeed, influence the relative humidity, assuming constant specific humidity. Assuming a typical specific humidity for the 500-hPa level in the dry area of 1×10^{-4} kg kg^{-1}, changing, modestly (like the interannual estimated variation using NCEP analysis), the local temperature from 265 to 266.5 K changes the relative humidity from 2.4% to 2.1%. In the moist case ($q \sim 2 \times 10^{-3}$ kg kg^{-1}) typically encountered in the ITCZ, the relative humidity would change from to 48.4% to 43.1%. These simple calculations confirm that the impact of temperature changes on the FTH are exacerbated over the moist area and that in dry conditions other mechanisms are needed to explain the relative humidity variability. Previous interannual analysis emphasized the role of El Niño in driving the interannual variability of UTH in the tropics (Bates et al. 2001; McCarthy and Toumi 2004), mainly through the use of EOF analysis. In this case, the first, and significant, mode is primarily driven by the absolute variation of the moist ITCZ over the Pacific and, hence, does not fully reflect the highly significant relative variability of the dry subtropics.

Over our area of interest, no direct relationship seems to hold with the El Niño index. Lateral mixing has been shown to have a strong contribution to the FTH relative humidity and is related to both extratropical jet dynamics and deep convection activity in the tropics. This

Downloaded from http://journals.ametsoc.org/jcli/article-pdf/22/24/6773/3951994/2009jcli2963_1.pdf by guest on 22 November 2020

finding is in agreement with previous theoretical studies identifying lateral mixing as a way to produce dry air (e.g., Pierrehumbert and Yang 1993; Pierrehumbert 1998; Galewsky et al. 2005). Trajectory results from the 2001 campaign survey of pollutants, Mediterranean Intensive Oxidant Study (MINOS), have highlighted the central role of Indian monsoon dynamics in the transport of pollutants in the Mediterranean upper troposphere (Lelieveld et al. 2002; Scheeren et al. 2003). When considering maps of the last-saturation coordinates (not shown), our computations also point toward the Indian monsoon area as one of the tropical sources of the air masses forming the tropical core of origin. The ''desert monsoon'' mechanism proposed by Rodwell and Hoskins (1996, 2001) suggests a dynamical link between the Indian monsoon convective activity and the subsiding area of the Mediterranean. The representation of theses two aspects in an atmospheric general circulation model (AGCM) is likely to be important for representing the interannual variability of the free tropospheric humidity over this region. Indeed, Brogniez et al. (2005) documented the behavior of a number of AGCMs participating in the Second Atmospheric Model Intercomparison Project (AMIP 2) exercise (Gates 1992) with respect to the FTH interannual variability. Most of the forced models ended up capturing this variability and, definitely, none were able to capture the chronology of the events from one year to another. These results were surprising in light of the conventional wisdom regarding humidity being driven by the large-scale dynamics, and one could have expected the GCM to reproduce these more easily. Besides the upper-level midlatitude jets, our results point to the role of Asian monsoon convection in shaping the the FTH distribution. A study of the same AMIP 2 models by Srinivasan (2003) indicates weak skill of the participating models in representing monsoon variability. We can speculate that this weak skill contributes to a poor representation of the tropical origin fraction of air masses that are linked to FTH variability at the interannual scale. Representation of breaks in the jet and other midlatitude upper-level dynamics could be another candidate to explain these previously reported model–observations differences (Waugh 2005; Cau et al. 2007). Further work on climate models hence should focus on these two topics to shed some light on the reasons for their agreement/failure to reproduce the observed humidity variability in the free troposphere.

While the focus of the present work is on a Northern Hemisphere area in summertime, significant interannual variability of FTH over other dry regions has also been identified. In boreal winter the dry edges of the oceanic ITCZ show large normalized variability that deserves further analysis, beyond of the scope of the present effort. The dry patch over the southern part of the Red Sea also reveals large variability that needs to be understood. In spring, similarly, the dry areas in both hemispheres, also not as dry as in the winter/summer climatology, exhibit significant variability at the interannual scale. A direct venue to complete the present work in the future concerns the detailed analysis of these variance enhanced regions using the current approach based on the 500-hPa proxy to assess the role of lateral mixing for these dry areas. Preliminary results from a broader ongoing study on the relative humidity distribution over the full intertropical belt indicates that the presently discussed lateral mixing process is repeatedly at play in the summer hemisphere dry subsiding areas and is exacerbated in boreal summer, presumably because of the configuration of the upper-levels jets in the northern midlatitudes. Another direct perspective of this study concerns the extension of the length of the FTH database to the recent Meteosat Second Generation water vapor measurements (Schmetz et al. 2002). Such an extended archive will be part of the climate Satellite Application Facility products in coming years (Schulz et al. 2008) and will offer an even longer documented period to assess the different mechanisms governing the interannual variability of the free tropospheric humidity.

Acknowledgments. Raymond Armante and the LMD/ARA team are greatly thanks for providing us their radiosondes archive. The authors are deeply indebted to R. T. Pierrehumbert for providing us with his model. The authors thank also Bernard Legras, LMD, for his comments that helped clarify some aspects of this work. The French ICARE center provided strong support for the extension of the database to the recent period and we especially thank Bruno Six for its dedicated support. We thank Karim Ramage from the Climserv data server from his help with the handling of the data and for providing the computational resources needed for this study. Finally the authors thank the two reviewers for their help in improving the final version of this paper. The CSR data are available via anonymous ftp from the Web site: http://climserv.ipsl.polytechnique.fr.

APPENDIX A

The Clear-Sky Radiance Archive

The Meteosat water vapor database has been recently extended from 1983–96 (Brogniez et al. 2006) to 2005 and now covers five versions of the Meteosat Visible and Infrared Imager (MVIRI) in operation onboard the fleet of satellites of the First Generation. Following Picon

Downloaded from http://journals.ametsoc.org/jcli/article-pdf/22/24/6773/3951994/2009jcli2963_1.pdf by guest on 22 November 2020

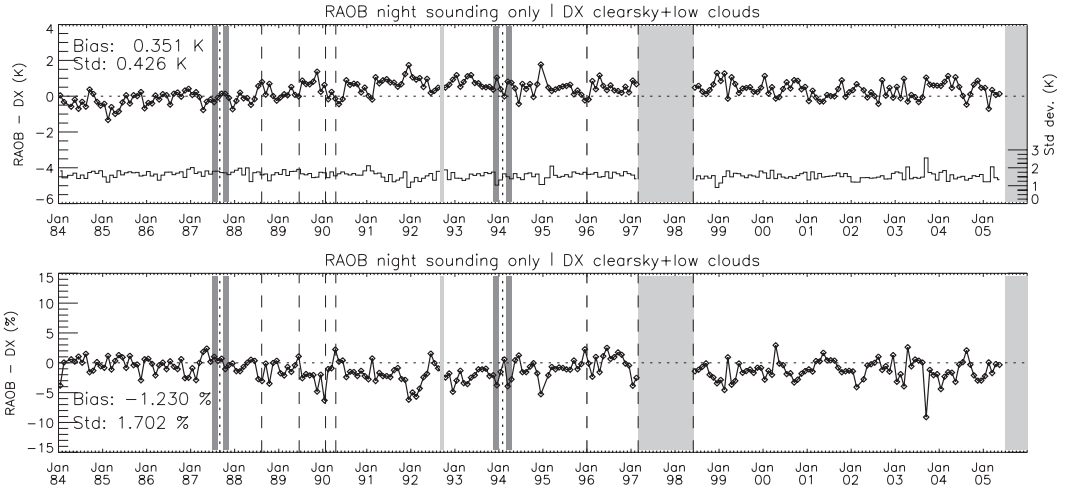


FIG. A1. (top) Comparisons between the Meteosat-5 WV brightness temperature simulations from radiosoundings using the RTTOV7 code and the observed BT (black line), with the main radiometric events (dashed lines) and the standard deviation (gray line) of the difference within each month (see Brogniez et al. 2006). (bottom) Comparisons between the FTH expected from radiosoundings (Jacobian-weighted relative humidity profile) and FTH observed from Meteosat (based on the FTH–BT algorithm). Gray shadings indicate missing values data (September 1992, and the Meteosat-6 period from March 1997 to June 1998); the mean bias and standard deviation are indicated.

et al. (2003), heterogeneities due to the successive radiometers (differences in the 6.3-μm filter functions) and the updates and improvements in the vicarious calibration technique used at the European Organization for the Exploitation of Meteorological Satellites (EUMETSAT) (Schmetz 1989; Van de Berg et al. 1995) have been corrected. In addition, a calibration adjustment is applied with respect to the one of HIRS-12/*NOAA-12*, which is assumed to be more accurate (e.g., Bréon et al. 2000). The present archive extends the work described in Brogniez et al. (2006) that concerned the Meteosat-2 to -5 measurements to most of the Meteosat-7 coverage (June 1998–June 2005). The period March 1997–May 1998, observed by the Meteosat-6 radiometer, is not introduced in this database owing to numerous instabilities in its calibration (more information available online at www.eumetsat.int), thus considered as missing.

Figure A1 (top) presents the comparison between the CSR dataset and the simulated BT of collocated radiosoundings extracted from the archive of the ECMWF as in Brogniez et al. (2006) (Uppala et al. 2005; R. Armante 2008, personal communication). The simulation of BTs was performed using the RTTOV-7 fast radiative code (Matricardi et al. 2004). Comparison is performed with the closest 0.625° × 0.625° satellite BT. Only nighttime soundings are conserved in the comparison [see Haimberger (2007) and references therein for the sounding problem during day time]. The small difference (0.351 K) between the BTs adjusted on HIRS-12/*NOAA-12* and the radiosonde BTs confirms the warm artificial bias of the Meteosat-5 water vapor channel, which has been highlighted in several works (Bréon et al. 2000; Sohn et al. 2000; Köpken et al. 2003). The small standard deviation of the difference ($\sigma = 0.426$ K) indicates good stability of the satellite archive with respect to the radiosonde archive throughout the period.

At the intraseasonal scale, and owing to some missing days in June for the years 1983 (availability of data starts on 17 July), 1984, 1987, and 1989 and because the dataset ends in June 2005, only the July–August months of the 1984–2004 period are preferred (20 years, summer 1997 excluded) to the longer summer season months (June–August), the latter being considered for a climatological description.

APPENDIX B

The Free-Tropospheric Humidity Database

The quantity FTH is determined from the following equation (Soden and Bretherton 1993):

$$\ln\left(\frac{p_0\langle \mathrm{RH}\rangle}{\cos\theta}\right) = a\mathrm{BT}_{6.3} + b, \qquad \text{(B1)}$$

which links $\langle \mathrm{RH}\rangle$; that is, the mean relative humidity (in percentage, defined with respect to water only) of a broad layer of the troposphere to the clear-sky 6.3-μm BT. This equation also makes use of a scaling parameter p_0, defined as the pressure of the 240-K isotherm

Downloaded from http://journals.ametsoc.org/jcli/article-pdf/22/24/6773/3951994/2009jcli2963_1.pdf by guest on 22 November 2020

normalized by a reference pressure of 300 hPa, and of a correction of the satellite viewing angle θ.

According to the related bibliography the vertical averaging operator $\langle\cdot\rangle$ can be:

i) the local relative humidity Jacobian ∂BT/∂RH, used in this study (e.g., Roca et al. 2003; Brogniez et al. 2004, 2005);
ii) the transmission-derived weighting function $\partial\tau/\partial \ln p$ (e.g., Schmetz and Turpeinen 1988; Stephens et al. 1996); or
iii) an idealized Jacobian ΔBT/ΔRH (e.g., Soden and Bretherton 1993; Jackson and Bates 2001).

The fitting parameters (a and b) of the BT to $\langle$RH$\rangle$ retrieval are determined once using a representative dataset of thermodynamic profiles extracted from ERA-40 and sampling the Meteosat field of view (30°N–30°S, 45°W–45°E).

Technically, estimates of p_0 were obtained from ERA-40 until 2002 and from the ECMWF operational analyses thereafter. Here p_0 is computed using spatially collocalized ECMWF temperature profiles (1.125°) and interpolated in time from the 6-hourly data for each 3-hourly CSR value. Tests with temperatures profiles from the NCEP–NCAR reanalyses (Kalnay et al. 1996) have shown little differences with the ECMWF-based computation of $p_0(\Delta p_0/p_0 \sim -0.02)$. Since $\Delta p_0/p_0$ scales ΔFTH/FTH, it turns this uncertainty into a small relative uncertainty of 2% in the estimation of FTH. Similarly, the use of local temperature profiles to compute p_0 has been preferred over the use of a climatological value to improve the retrieval at the dry end of the spectrum. For example, there is a 6% difference between the mean p_0 of July 1992 and the value for the 1983–2004 period (averaged over the Meteosat field of view). This yields up to 6% (absolute) uncertainty in dry atmospheres (FTH $< 20\%$) and 1.3% in moist regimes (FTH $> 50\%$).

As for the CSR, the FTH is compared to the ECMWF radiosonde archive in Fig. A1 (bottom). The FTH is derived from the radiosondes using the RTTOV Jacobian (with the temperature and humidity profiles as inputs) and by vertically averaging the relative humidity profile with the Jacobian. As for the BT evaluation, the comparison highlights high consistency of the FTH satellite product, which is stable over time. Complimentary analyses at the sonde scale (no spatial/temporal average) support this consistency.

REFERENCES

Allan, R., 2006: Variability in clear-sky longwave radiative cooling of the atmosphere. *J. Geophys. Res.,* **111,** D22105, doi:10.1029/2006JD007304.

Bates, J., X. Wu, and D. Jackson, 2001: Interannual variability of upper tropospheric water vapor band brightness temperature. *J. Climate,* **9,** 427–438.

Bhat, G. S., 2006: The Indian drought of 2002: A subseasonal phenomenon? *Quart. J. Roy. Meteor. Soc.,* **132,** 2583–2602.

Bock, O., F. Guichard, S. Janicot, J.-P. Lafore, M.-N. Bouin, and B. Sultan, 2007: Multiscale analysis of precipitable water vapor over Africa from GPS data and ECMWF analyses. *Geophys. Res. Lett.,* **34,** L09705, doi:10.1029/2006GL028039.

Bony, S., and Coauthors, 2006: How well do we understand and evaluate climate change feedback processes? *J. Climate,* **19,** 3445–3482.

Bréon, F.-M., D. Jackson, and J. Bates, 2000: Calibration of the METEOSAT water vapor channel using collocated NOAA/HIRS-12 measurements. *J. Geophys. Res.,* **105,** 11 925–11 933.

Brogniez, H., and R. T. Pierrehumbert, 2006: Using microwave observations to assess large-scale control of the free tropospheric water vapor in the mid-latitudes. *Geophys. Res. Lett.,* **33,** L14801, doi:10.1029/2006GL026240.

——, R. Roca, and L. Picon, 2004: Interannual and intraseasonal variabilities of the free tropospheric humidity using METEOSAT water vapor channel over the tropics. *Proc. Eumetsat Meteorological Satellite Conf.,* Prague, Czech Republic, Eumetsat.

——, ——, and ——, 2005: Evaluation of the distribution of subtropical free tropospheric humidity in AMIP-2 simulations using METEOSAT water vapor channel data. *Geophys. Res. Lett.,* **32,** L19708, doi:10.1029/2005GL024341.

——, ——, and ——, 2006: A clear-sky radiance archive from Meteosat ''water vapor'' observations. *J. Geophys. Res.,* **111,** D21109, doi:10.1029/2006JD007238.

Cau, P., J. Methven, and B. Hoskins, 2007: Origins of dry air in the tropics and subtropics. *J. Climate,* **20,** 2745–2759.

Chung, E.-S., B.-J. Sohn, J. Schmetz, and M. Koenig, 2007: Diurnal variation of upper tropospheric humidity and its relations to convective activities over tropical Africa. *Atmos. Chem. Phys.,* **7,** 351–381.

Elliot, W., and D. Gaffen, 1991: On the utility of radiosonde humidity archives for climate studies. *Bull. Amer. Meteor. Soc.,* **72,** 1507–1520.

Emanuel, K., 1991: A scheme for representing cumulus convection in large-scale models. *J. Atmos. Sci.,* **45,** 2313–2335.

Fischer, H., N. Eigenwillig, and H. Müller, 1981: Information content of METEOSAT and Nimbus/THIR water vapor channel data: Altitude association of observed phenomena. *J. Appl. Meteor.,* **20,** 1344–1352.

Galewsky, J., A. Sobel, and I. Held, 2005: Diagnosis of subtropical humidity dynamics using tracers of last saturation. *J. Atmos. Sci.,* **62,** 3353–3367.

Gates, W., 1992: AMIP: The Atmospheric Model Intercomparison Project. *Bull. Amer. Meteor. Soc.,* **73,** 1962–1970.

Gettelman, A., W. Collins, E. Fetzer, A. Eldering, F. Irion, P. Duffy, and G. Bala, 2006: Climatology of upper-tropospheric relative humidity from the Atmospheric Infrared Sounder and implications for climate. *J. Climate,* **19,** 6104–6121.

Haimberger, L., 2007: Homogenization of radiosonde temperature time series using innovation statistics. *J. Climate,* **20,** 1377–1403.

Jackson, D., and J. Bates, 2001: Upper tropospheric humidity algorithm assessment. *J. Geophys. Res.,* **106D,** 32 259–32 270.

Kalnay, E., and Coauthors, 1996: The NCEP/NCAR 40-Year Reanalysis Project. *Bull. Amer. Meteor. Soc.,* **77,** 437–471.

Köpken, C., J.-N. Thépaut, and G. Kelly, 2003: Assimilation of geostationary WV radiances from GOES and METEOSAT at ECMWF. Research Rep. 14, Eumetsat/ECMWF, 30 pp.

Downloaded from http://journals.ametsoc.org/jcli/article-pdf/22/24/6773/3951994/2009jcli2963_1.pdf by guest on 22 November 2020

Lelieveld, J., and Coauthors, 2002: Global air pollution crossroads over the Mediterranean. *Science,* **298,** 794–799.

Luo, Z., D. Kley, and R. Johnson, 2007: Ten years of measurements of tropical upper- tropospheric water vapor by MOZAIC. Part I: Climatology, variability, transport, and relation to deep convection. *J. Climate,* **20,** 418–435.

Manabe, S., and R. Wetherald, 1967: Thermal equilibrium of the atmosphere with a given distribution of relative humidity. *J. Atmos. Sci.,* **24,** 241–249.

Mapes, B., 2001: Water's two height scales: The moist adiabat and the radiative troposphere. *Quart. J. Roy. Meteor. Soc.,* **127,** 2353–2366.

Matricardi, M., F. Chevallier, G. Kelly, and J.-N. Thépaut, 2004: An improved general fast radiative transfer model for the assimilation of radiance observations. *Quart. J. Roy. Meteor. Soc.,* **130,** 153–173.

McCarthy, M., and R. Toumi, 2004: Observed interannual variability of the tropical troposphere relative humidity. *J. Climate,* **17,** 3181–3191.

Mote, P., H. Clark, T. Dunkerton, R. Harwood, and H. Pumphrey, 2000: Intraseasonal variations of water vapor in the tropical upper troposphere and tropopause region. *J. Geophys. Res.,* **105D,** 17 457–17 470.

Peixoto, J., and A. Oort, 1996: The climatology of relative humidity in the atmosphere. *J. Climate,* **9,** 3443–3463.

Picon, L., S. Fongang, G. Seze, and M. Desbois, 1995: African and Atlantic short-term climatic variations described from METEOSAT water vapor channel. *Ann. Geophys.,* **13,** 768–781.

——, R. Roca, S. Serrar, and M. Desbois, 2003: A new METEOSAT ''water vapor'' archive for climate studies. *J. Geophys. Res.,* **108,** 4301, doi:10.1029/2002JD002640.

Pierrehumbert, R. T., 1995: Thermostats, radiator fins, and the local runaway greenhouse. *J. Atmos. Sci.,* **52,** 1784–1806.

——, 1998: Lateral mixing as a source of subtropical water vapor. *Geophys. Res. Lett.,* **25,** 151–154.

——, 1999: Subtropical water vapor as a mediator of rapid global climate change. *Mechanisms of Global Change at Millennial Time Scales, Geophys. Monogr.,* Vol. 112, Amer. Geophys. Union.

——, and H. Yang, 1993: Global chaotic mixing of isentropic surfaces. *J. Atmos. Sci.,* **50,** 2462–2480.

——, and R. Roca, 1998: Evidence for control of Atlantic subtropical humidity by large-scale advection. *Geophys. Res. Lett.,* **25,** 4537–4540.

——, H. Brogniez, and R. Roca, 2007: On the relative humidity of the Earth's atmosphere. *The Global Circulation of the Atmosphere,* T. Schneider and A. Sobel, Eds. Princeton University Press, 143–185.

Redelsperger, J.-L., A. Diongue, A. Diedhiou, J.-P. Ceron, M. Diop, J.-F. Gueremy, and J.-P. Lafore, 2002: Multi-scale description of a Sahelian synoptic weather system representative of the West African Monsoon. *Quart. J. Roy. Meteor. Soc.,* **128,** 1229–1257.

Roca, R., M. Viollier, L. Picon, and M. Desbois, 2002: A multisatellite analysis of deep convection and its moist environment over the Indian Ocean during the winter monsoon. *J. Geophys. Res.,* **107,** 8012, doi:10.1029/2000JD000040.

——, H. Brogniez, L. Picon, and M. Desbois, 2003: Free tropospheric humidity observations from Meteosat water vapor channel data. Preprints, *17th Conf. on Hydrology,* Long Beach, CA, Amer. Meteor. Soc., CD-ROM, J3.7.

——, J.-P. Lafore, C. Piriou, and J.-L. Redelsperger, 2005a: Extratropical dry-air intrusion into the West African monsoon midtroposphere: An important factor for the convective activity of the Sahel. *J. Atmos. Sci.,* **62,** 390–407.

——, S. Louvet, L. Picon, and M. Desbois, 2005b: A study of convective systems, water vapor and top of the atmosphere cloud radiative forcing over the Indian Ocean using INSAT-1B and ERBE data. *Meteor. Atmos. Phys.,* **90,** doi:10.1007/s00703-004-0098-3.

Rodwell, M., and B. Hoskins, 1996: Monsoon and the dynamics of deserts. *Quart. J. Roy. Meteor. Soc.,* **122,** 1385–1404.

——, and ——, 2001: Subtropical anticyclones and summer monsoons. *J. Climate,* **14,** 3192–3211.

Rossow, W., and R. Schiffer, 1991: ISCCP cloud data products. *Bull. Amer. Meteor. Soc.,* **72,** 2–20.

Ryoo, J.-M., D. Waugh, and A. Gettelman, 2008: Subtropical upper tropospheric humidity. *Atmos. Chem. Phys.,* **8,** 2643–2655.

Salathé, E., and D. Hartmann, 1997: A trajectory analysis of tropical upper-tropospheric moisture and convection. *J. Climate,* **10,** 2533–2547.

Sassi, F., M. Salby, H. Pumphrey, and W. Read, 2002: Influence of the Madden–Julian Oscillation on upper tropospheric humidity. *J. Geophys. Res.,* **107,** 4681, doi:10.1029/2001JD001331.

Scheeren, H., and Coauthors, 2003: The impact of monsoon outflow from India and Southeast Asia in the upper troposphere over the eastern Mediterranean. *Atmos. Chem. Phys.,* **3,** 2285–2330.

Schmetz, J., 1989: Operational calibration of the Meteosat water vapor channel by calculated radiances. *Appl. Opt.,* **28,** 3030–3038.

——, and O. Turpeinen, 1988: Estimation of the upper tropospheric relative humidity field from Meteosat water vapor image data. *J. Appl. Meteor.,* **27,** 889–899.

——, C. Geijo, W. Menzel, K. Strabala, L. Van de Berg, K. Holmlund, and S. Tjemkes, 1995: Satellite observations of upper tropospheric humidity, clouds and wind field divergence. *Beitr. Phys. Atmos.,* **68,** 354–357.

——, P. Pili, S. Tjemkes, D. Just, S. Rota, and A. Ratier, 2002: An introduction to Meteosat Second Generation (MSG). *Bull. Amer. Meteor. Soc.,* **83,** 977–992.

Schulz, J., and Coauthors, 2008: Operational climate monitoring from space: The Eumetsat satellite application facility on climate monitoring (CM-SAF). *Atmos. Chem. Phys.,* **8,** 8517–8563.

Sherwood, S., 1996: Maintenance of the free-tropospheric tropical water vapor distribution. Part II: Simulation by large-scale advection. *J. Climate,* **9,** 2919–2934.

——, and C. Meyer, 2006: The general circulation and robust relative humidity. *J. Climate,* **19,** 6278–6290.

——, E. Kursinski, and W. Read, 2006: A distribution law for free tropospheric relative humidity. *J. Climate,* **19,** 6267–6277.

Soden, B., and F. Bretherton, 1993: Upper tropospheric relative humidity from the GOES 6.7μm channel: Method and climatology for July 1987. *J. Geophys. Res.,* **98D,** 16 669–16 688.

——, and J. Lanzante, 1996: An assessment of satellite and radiosonde climatologies of upper-tropospheric water vapor. *J. Climate,* **9,** 1235–1250.

Sohn, B.-J., and J. Schmetz, 2004: Water vapor–induced OLR variations associated with high cloud changes over the tropics: A study from *Meteosat-5* observations. *J. Climate,* **17,** 1987–1996.

——, ——, S. Tjemkes, M. Koenig, H. Lutz, A. Arriaga, and E. Chung, 2000: Intercalibration of the METEOSAT-7 water vapor channel with SSM/T-2. *J. Geophys. Res.,* **105D,** 15 673–15 680.

Downloaded from http://journals.ametsoc.org/jcli/article-pdf/22/24/6773/3951994/2009jcli2963_1.pdf by guest on 22 November 2020

——, ——, and E.-S. Chung, 2008: Moistening processes in the tropical upper troposphere observed from Meteosat measurements. *J. Geophys. Res.,* **113,** D13109, doi:10.1029/2007JD009527.

Spencer, R., and W. Braswell, 1997: How dry is the tropical free troposphere? Implications for a global warming theory. *Bull. Amer. Meteor. Soc.,* **78,** 1097–1106.

Srinivasan, J., 2003: Diagnostic study of errors in the simulation of tropical continental precipitation. *Ann. Geophys.,* **21,** 1197–1207.

Stephens, G., and T. Greenwald, 1991: The Earth's radiation budget and its relation to atmospheric hydrology. 1. Observations of the clear-sky greenhouse effect. *J. Geophys. Res.,* **96D,** 15 311–15 324.

——, D. Jackson, and I. Wittmeyer, 1996: Global observations of upper tropospheric water vapor derived from TOVS radiance data. *J. Climate,* **9,** 305–326.

Tian, B., B. Soden, and X. Wu, 2004: Diurnal cycle of convection, clouds, and water vapor in the tropical upper troposphere: Satellites versus a general circulation model. *J. Geophys. Res.,* **109,** D10101, doi:10.1029/2003JD004117.

Udelhofen, P., and D. Hartmann, 1995: Influence of tropical cloud systems on the relative humidity in the upper troposphere. *J. Geophys. Res.,* **100,** 7423–7440.

Uppala, S., and Coauthors, 2005: The ERA-40 Re-Analysis. *Quart. J. Roy. Meteor. Soc.,* **131,** 2961–3012.

Van de Berg, L., J. Schmetz, and J. Whitlock, 1995: On the calibration of the Meteosat water vapor channel. *J. Geophys. Res.,* **100,** 21 069–21 076.

Waugh, D., 2005: Impact of potential vorticity intrusions on subtropical upper tropospheric humidity. *J. Geophys. Res.,* **110,** D11305, doi:10.1029/2004JD005664.

Zender, C. S., 1999: Global climatology of abundance and solar absorption of oxygen collision complexes. *J. Geophys. Res.,* **104D,** 24 471–24 484.

Zhan, R., J. Li, and A. Gettelman, 2006: Intraseasonal variations of upper tropospheric water vapor in Asian monsoon region. *Atmos. Chem. Phys. Discuss.,* **6,** 8069–8095.

Downloaded from http://journals.ametsoc.org/jcli/article-pdf/22/24/6773/3951994/2009jcli2963_1.pdf by guest on 22 November 2020